PARTICLE FILTER BASED MULTI-SENSOR FUSION FOR SOLVING LOW FREQUENCY ELECTROMAGNETIC NDE INVERSE PROBLEMS

Tariq Khan[1], Pradeep Ramuhalli[1] (IEEE senior member) and
Sarat Dass[2]
[1]Dept. of Electrical and Computer Engineering, [2]Dept. of Statistics and Probability
Michigan State University, East Lansing, MI 48824
khantari,sdass@msu.edu, r.pradeep@ieee.org

Abstract:

Flaw profile characterization from NDE measurements is a typical inverse problem. A novel transformation of this inverse problem into a tracking problem, and subsequent application of a sequential Monte Carlo method called particle filtering, has been proposed by the authors in an earlier publication [1]. In this study, the problem of flaw characterization from multi-sensor data is considered. The NDE inverse problem is posed as a statistical inverse problem and particle filtering is modified to handle data from multiple measurement modes. The measurement modes are assumed to be independent of each other with principal component analysis (PCA) used to legitimize the assumption of independence. The proposed particle filter based data fusion algorithm is applied to experimental low frequency NDE data to investigate its feasibility.

Index Terms— **Inverse Problems, Nondestructive Evaluation, Particle Filters, Data Fusion**

1. INTRODUCTION

The estimation of flaw depth profiles (i.e., the sequence of flaw depths as a function of spatial position) from nondestructive evaluation (NDE) measurements is a typical inverse problem. This inverse problem is ill-posed due to non-uniqueness of the solution, particularly in the presence of measurement noise. Various techniques have been proposed in the literature to address ill-posedness [2]. Direct approaches for solving NDE inverse problems typically rely on the use of signal processing techniques to establish a relationship between specific characteristics of the signal and the geometry of the defect, ignoring the underlying physical process. These methods typically pose the inverse problem as determining a mapping from the measurement space to the material property space [3-4] where the set of unknown parameters that define the mapping are

determined from measurements. Direct approaches ranging from calibration methods to more recent procedures based on neural networks [5-6] have been proposed. The advantages of this approach are their simplicity and speed; however, the approaches are very sensitive to the analytical models that are used as well as noise in the measurements. Iterative methods, on the other hand, usually rely on a physical model to accurately simulate the underlying physical phenomenon and predict the probe response [7]. The model is used to estimate the measurement given the flaw profile, which is iteratively derived by minimizing the difference between the estimated and actual measurements. Minimization may be through conventional techniques such as conjugate gradient, though other techniques such as simulated annealing [8] or genetic algorithms [9] have been proposed. Numerical models such as a finite element model or integral equation models [3], [6], [9-21] have been proposed for electromagnetic NDE signal inversion, and though accurate, tend to be computationally expensive since the models must be solved iteratively. A Bayesian technique was also proposed for defect signal analysis in NDE images [22-23], where a hierarchical Bayesian framework was designed for detecting and estimating NDE defect signals from noisy measurements.

The use of multiple inspection modes is becoming common in various NDE applications. The availability of information from multiple measurement modes has the potential for improving the accuracy and reliability in flaw profiling due to complementary information contained in multiple sensors. However, this requires development of computationally efficient data fusion techniques for solving inverse problems when multiple measurements are available. Many researchers have employed data fusion techniques to solve the NDE inverse problem [24-25]. Commonly proposed solutions include neural networks [26-29], Bayesian analysis based on Dempster-Shafer evidence theory [30-32], wavelet and other multi-resolution algorithms [29], and image fusion [31,34,35] in time and frequency domain. These methods have been applied to fuse NDE data from a range of sources, including multifrequency eddy current measurements (ECT) [25,26,28], ECT data and ultrasound measurements [26-28,34-35], ultrasound, x-ray and acoustic emission measurements [32], and other techniques (such as pulsed eddy current measurements) [36]. In addition to these conventional fusion

techniques, other methods such as the Q-transform based technique [37] have also been recently investigated.

Available fusion algorithms are generally based on processing signals or images without regard to physics of the measurement process. Further, most of the proposed techniques ~~also~~ have drawbacks in terms of lower accuracy of inversion and high computational cost. In order to address these drawbacks, the authors have proposed a sequential Monte Carlo based method for solution of low-frequency NDE inverse problems [1]. In this study, the sequential Monte Carlo technique is extended to fusing NDE data from multiple NDE measurement modes.

The rest of this paper is organized as follows. The next section describes the problem formulation for NDE inverse problem in terms of a recursive framework in the presence of measurement data from multiple measurement modes. The particle filtering technique followed by its application for solving the NDE inverse problem in the presence of multiple measurement modes is discussed. The particle filter based data fusion technique is developed assuming that NDE measurement modes are uncorrelated to each other. The use of principal component analysis (PCA) to legitimize the assumption of independence of measurement modes is then discussed. Results of flaw profiling from multimodal NDE measurements are presented to validate the proposed techniques. A comparative study of flaw profiling results when using a single measurement mode, and data fusion with/without PCA, is also reported in this paper. Finally, conclusions and future work are presented. The notations used in the manuscript are tabulated in table 1 for clarity.

2. NDE INVERSE PROBLEM FORMULATION

a. Problem Formulation

The problem formulation described here is applicable to flaw profile reconstruction in both two and three dimensions (2D and 3D). The 2D problem is equivalent to estimating the flaw depths along the length of the specimen (where the depth along the width dimension is assumed to be invariant). In this case, the length of specimen is divided into K locations. The 3D problem is equivalent to estimating the flaw

depth at each location on the specimen surface, and therefore, the surface of the specimen is divided into *K* discrete locations. In each case, flaw depth is the unknown at each discretized location. Examples of the formulation for 2D (crack-like) and 3D (volumetric flaws such as corrosion, wear or wall thickness loss) profiling are shown in Figures 1 and 2 respectively. The depth profile of flaws in the specimen (2D or 3D) is expressed in terms of a set $\vec{X} = \{x_1, x_2, ...x_{k-1}, x_k, x_{k+1}, ...x_{K-1}, x_K\}$, where the each element x_k of the set is state (flaw depth) at the discrete location k. Assume that measurements $\bar{z}_k = \{z_k^1, z_k^2, ..., z_k^q, ..., z_k^Q\} = \{z_k^q \mid q = 1:Q\}$ from Q measurement modes are available at each position index k ($1 \le k \le K$). The evaluation of the sequence of states given the set of measurements is the inverse problem. This inverse problem can be formulated in terms of a statistical estimation problem. In this case, the unknown parameter is the set of states $\vec{X}$ while the corresponding observation is the set of measurements $\vec{Z} = \{z_1^1, z_1^2, ...z_1^Q, z_2^1, ...z_k^q, ...z_K^Q\}$. The posterior PDF $p(\vec{X} \mid \vec{Z})$ of the states $\vec{X}$ for each measurement mode q can be computed in the framework of statistical inverse problems [38]. The states $\vec{X}$ are estimated from the posterior PDF:

$$p(\vec{X} \mid \vec{Z}) \propto p(\vec{Z} \mid \vec{X})\, p(\vec{X}) \tag{1}$$

Here $p(\vec{Z} \mid \vec{X})$ is the likelihood function and $p(\vec{X})$ captures available prior information about the set of states (set of flaw depths). The estimation of $p(\vec{Z} \mid \vec{X})$ is generally a computationally expensive process due to the high dimensionality of the state vector $\vec{X}$. Evaluating the posterior PDF sequentially (i.e., at each position by stepping through the position index *k*) can potentially keep the computational cost and complexity of the inverse problem low. Three conditions, which are fundamental to the proposed problem formulation, are assumed to enable the sequential solution to the inverse problem [38]. Firstly a locally dependent Markov field is adopted to solve the problem. This Markovian assumption has been shown to be valid for low-frequency

electromagnetic NDE (magnetostatic and eddy current) [39]. Therefore, the relationship offered by (1) holds locally and the equation can also be written for a neighborhood N_k around the position index k, where $1 \le k \le K$:

$$p(x_k \mid \{\bar{z}_j \mid j \in N_k\}) \propto p(\{\bar{z}_j \mid j \in N_k\} \mid x_k).p(x_k) \quad (2)$$

The neighborhood elements N_k of each discretized location for a 2D problem are given by a 1D window $x_{k-(2L+1):k-1,k+1:k+(2L+1)}$ as shown in figure 1. L is a scalar parameter which controls the size of the neighborhood. N_k for each location for a 3D problem are defined by a 2D window on the surface of specimen $x_{p,q}\big|_{\substack{p=m-(2L+1):m-1,m+1:m+(2L+1),\\ q=n-(2L+1):n-1,n+1:n+(2L+1)}}$ as shown in Figure 2. The neighborhood as defined here is similar to the lexicographic arrangement of pixels commonly used in the image processing literature [40].

The second assumption is that the observations (measurements) are mutually independent within the neighborhood of the state given true values of the unknown states:

$$p(\{\bar{z}_j \mid j \in N_k\} \mid x_k) = \prod_{j \in N_k} p(\bar{z}_j \mid x_j) \quad (3)$$

Finally, the prior density of the unknown state is assumed to be a product of exponential densities centered on the value of the states in the neighborhood:

$$p(x_k \mid x_j\big|_{\substack{j \in N_k \\ j \neq k}}) = e^{-\sum_{j \in N_k} \frac{\left\| x_j - x_k \right\|^p}{p}}, \quad (4)$$

where p is a scalar, with value selected to be around 1 to ensure a low amount of variability in the state value within the neighborhood, and $x_j\big|_{\substack{j \in N_k \\ j \neq k}}$ are the states in the neighborhood N_k of location k. The assumptions specified by (3) and (4) simplify computation for local Markov fields [38].

b. The Inverse Problem as a Tracking Problem

As discussed earlier, the inverse problem in NDE is to determine the best flaw characteristics that match the measurements. The inverse problem may be modeled using two sets of equations [41] – a state transition equation that is used to model the evolution of the states with respect to spatial position

$$x_k = f_k(x_j \mid_{\substack{j \in N_k \\ j \neq k}}, \nu_k) \Leftrightarrow p(x_k \mid x_j \mid_{\substack{j \in N_k \\ j \neq k}}) \quad , \tag{5}$$

and measurement models that relate the measurements from multiple sensors to the states at a given position:

$$z_k = h_k^q(x_k, \mu_k^q) \Leftrightarrow p(z_k \mid x_k) \quad , \tag{6}$$

where f_k and h_k^q are functions that model the state transition process and the measurement process respectively, and ν_k and μ_k^q represent the process noise and measurement noise respectively. Note that the state transition and measurement equations are applied to the local neighborhood of state x_k. The problem described by equations (5) and (6) is often referred to as a tracking problem, and is used frequently in target tracking applications [41-42]. In these applications, the state transition function models the motion of a target from a known position x_j, while the measurement function describes some function of the target position. Process and measurement noise densities represent the uncertainty in the state and measurement models. The tracking problem as defined in equations (5) and (6) is a dynamic state estimation problem [41]. The Bayesian approach to this problem is to construct a posterior PDF of the state, based on the sequence of measurements.

The problem described by equations (5) and (6) can be shown to be equivalent to the statistical inverse problem defined by equation (1) by the following arguments. The state transition function (when taken with the associated process noise distribution) is equivalent to the local prior PDF used in the statistical inverse problem. Similarly the measurement function is equivalent to the local likelihood PDF in the statistical inverse problem when a locally independent Markov field is assumed (sec. 2a). The equivalence

of tracking problem to statistical probabilities is also shown in equations (5&6). The advantage of this equivalence is the potential applicability of solution techniques for tracking problems to solve the NDE inverse problem. Note also that the formulation of the inverse problem as a statistical inverse problem (1) or equivalently, as a tracking problem as in equations (5) and (6), implicitly assumes that the NDE measurement process is a localized process, i.e., the measurement at a particular location k is only affected by the state of the sample in a neighborhood of k. As mentioned earlier, the Markovian assumption is valid for low-frequency electromagnetic NDE (magnetostatic and eddy current NDE) [40] provided the neighborhood is selected appropriately.

3. APPLICATION OF PARTICLE FILTERS TO SOLVE NDE INVERSE PROBLEMS USING MULTIPLE MODE MEASUREMENT DATA

a. Solutions to the Tracking Problem

Kalman filtering [41] provides an optimal solution to the tracking problem if the following two conditions are met:

(i) The function which relates the states in a neighborhood (i.e., the state transition function) and the function which relates the state to measurement (i.e., the measurement function) are linear.

(ii) The likelihood and prior PDFs are Gaussian.

In general, for the NDE inverse problem, these functions can be non-linear and the PDFs can be non Gaussian (multi-modal). Therefore, the Kalman filter cannot provide an optimal solution and suboptimal algorithms may be necessary to evaluate the flaw depth. Therefore, a more generalized filtering technique is required to solve this inverse problem. Particle filters offer such a generalized filtering technique.

b. Theory of Particle Filters

Particle filters are sequential Monte Carlo methods based on point mass (or "particle") representations of probability densities that can be applied to any state-space model and which generalize traditional Kalman filtering methods [41-42]. In this approach to dynamic state estimation, the posterior probability density function (PDF) of the state is constructed based on all available information, including the set of received measurements. A brief description of the particle filter algorithm is provided next. To

simplify the discussion, we assume that measurements $z_k = \{z_k^q \mid q = 1\} \equiv z_k$ from a single measurement mode (i.e., $Q = 1$) are available. This assumption will be relaxed in the next section, where we extend the particle filtering framework to incorporate multimodal measurements.

With the assumption of a single measurement mode (and temporarily simplifying the notation by dropping the superscript q), the PDF of the state x_k conditioned on all measurements up to (and including z_k), $p(x_k, z_{1:k})$ may be obtained recursively in two stages: prediction and update. The prediction stage uses the system model to predict the PDF forward from one measurement location to the next. Suppose that the required PDF $p(x_k \mid z_{1:k-1})$ at location $k-1$ is available. The prediction stage involves using the system model to obtain the prediction density of the state at k via the Chapman-Kolmogorov equation [41]:

$$p(x_k \mid z_{1:k-1}) = \int p(x_k \mid x_{k-1}) p(x_{k-1} \mid z_{1:k-1}) dx_{k-1}. \tag{7}$$

If we consider a Markov process of order one, then $p(x_k \mid x_{k-1}, z_{1:k-1}) = p(x_k \mid x_{k-1})$. Since the state is usually subject to unknown disturbances (modeled as random noise), the prediction step generally translates, deforms, and otherwise distorts the PDF. The update operation uses the latest measurement to modify the prediction PDF. This is achieved using Bayes' theorem as follows:

$$p(x_k \mid z_k) = p(x_k \mid z_k, z_{1:k-1}) = \frac{p(z_k \mid x_k, z_{1:k-1}) p(x_k \mid z_{1:k-1})}{p(z_k \mid z_{1:k-1})} \tag{8}$$

$$= \frac{p(z_k \mid x_k) p(x_k \mid z_{1:k-1})}{p(z_k \mid z_{1:k-1})},$$

where the normalizing constant is given by:

$$p(z_k \mid z_{1:k-1}) = \int p(z_k \mid \vec{X}) p(\vec{X} \mid z_{1:k-1}) dx_k. \tag{9}$$

In order to apply particle filtering, the desired posterior PDF is represented in terms of samples and associated weights at each location. In order to develop the details of the algorithm, let $\{x_k^i, w_k^i\}|_{1:Ns}$ denote a random measure that characterizes the posterior PDF at location k. x_k^i are the set of support points with associated weights w_k^i and $i = 1: N_s$ is the total number of samples used. The weights are normalized such that $\sum_{i=1}^{N_s} w_k^i$. Then, the posterior density at k can be approximated as [41]

$$p(x_k \mid z_k) \approx \sum_{i=1}^{N_s} w_k^i \delta(x_k - x_k^i). \tag{10}$$

Normalized weights are chosen using the principle of importance sampling [41]. According to this principle, suppose $p(x) \propto \pi(x)$ is a probability density from which it is difficult to draw samples but for which $\pi(x)$ can be evaluated and samples can be drawn from $\pi(x)$. In addition, let x^i be samples that are easily generated from a proposal $q(.)$ called an *importance density*. Then, a weighted approximation to the density $p(x)$ is given by

$$p(x) \approx \sum_{i=1}^{N_s} w^i \delta(x - x^i), \tag{11}$$

where $w^i \propto \frac{\pi(x^i)}{q(x^i)}$ is the normalized weight of the *i*th particle. Therefore, if the samples x_k^i were drawn from an importance density $q(x_{1:k} \mid z_{1:k})$, the weights are given by [41]

$$w_k^i \propto \frac{p(x_{1:k}^i \mid z_{1:k})}{q(x_{1:k}^i \mid z_{1:k})}. \tag{12}$$

With the reception of measurement z_k at position k, we wish to approximate $p(x_{1:k} \mid z_{1:k})$ with a new set of samples. Given the set of weights w_{k-1} at position $k-1$, the weights at position k may be computed recursively using the weight update equation derived from the principle of importance sampling as

$$w_k^i \propto w_{k-1}^i \frac{p(z_k \mid x_k^i) p(x_k^i \mid x_{k-1}^i)}{q(x_k^i \mid x_{k-1}^i, z_k)}. \quad (13)$$

The most commonly used variant of particle filter, sampling important re-sampling (SIR) algorithm [42] is used in this study. The importance density in the SIR algorithm is chosen as the transitional prior

$$q(x_k^i \mid x_{k-1}^i, z_k) = p(x_k^i \mid x_{k-1}^i). \quad (14)$$

Therefore from (12) and (13),

$$w_k^i \propto w_{k-1}^i p(z_k \mid x_k^i). \quad (15)$$

We can also write (14) as

$$w_k^i \propto p(z_k \mid x_k^i) \quad (16)$$

c. Particle filtering for Multisensor Data Fusion

When multiple measurement modes are available, likelihood PDFs corresponding to each measurement mode need to be considered in weight assignment to the sample. Assume that $w_k^{i,q}$ is the weight of the sample i at position index k assigned by individual measurement mode q. For every sample at each position index, Q weights are therefore computed using the respective likelihood PDFs. The likelihood function corresponding to the q^{th} measurement mode is given by (16):

$$w_k^{i,q} \propto p(z_k^q \mid x_k^i). \quad (17)$$

If the measurement processes are assumed to be independent, then the joint likelihood due to measurement modes $q = 1,2,.....,Q$ is the product of likelihoods for individual measurement modes:

$$p(z_k \mid x_k^i) = p(z_k^1 \mid x_k^i).p(z_k^2 \mid x_k^i).,.....,.p(z_k^Q \mid x_k^i). \tag{18}$$

Therefore, from (17) and (18), we get

$$w_k^i \propto p(z_k^1 \mid x_k^i).p(z_k^2 \mid x_k^i)..... p(z_k^Q \mid x_k^i). \tag{19}$$

Using (16) and (19), the final weight assigned to sample i at position index k is

$$w_k^i \propto w_k^{i,1}, w_k^{i,2}, ..., w_k^{i,Q}. \tag{20}$$

As mentioned above, it is assumed that the measurement processes are independent. However, the measurement processes may be correlated, and the assumption of independence is not valid in that case. In order to make the assumption of independence more legitimate, the principal component analysis (PCA) technique is applied to data from different measurement modes. PCA [43] is mathematically defined as an orthogonal linear transformation that transforms the data to a new coordinate system. PCA can also be applied to data from multiple measurement modes. At each position index k, the measurements $z_j^{1:Q}|_{j \in N_k}$ within its neighborhood from all measurement modes $(1:Q)$ are considered. This multidimensional data is now the input of PCA technique. The following steps are carried out to evaluate the principal components.

Step 1: The multi-sensor measurements $z_j^{1:Q}|_{j \in N_k}$ are stored as a vector $\varsigma^q|_{q=1:Q}$, where each measurement mode is assumed to be one component of the vector.

Step 2: The data vector is adjusted by subtracting out its mean.

$$\varsigma^q = \varsigma^q - mean(\varsigma^q). \tag{21}$$

Step 3: The adjusted data vectors are arranged as rows of a matrix. This newly formed matrix will be called the “adjusted data matrix”.

$$\varsigma = [\varsigma^1, \varsigma^2, ..., \varsigma^Q]. \quad (22)$$

Step 4: The covariance matrix of the "adjusted data matrix" is computed:

$$\sigma^q = \mathrm{cov}(\varsigma^q). \quad (23)$$

Step 5: Eigenvectors λ^q of the covariance matrix are then evaluated:

$$\lambda^q = eig(\sigma^q). \quad (24)$$

Step 6: The computed eigenvectors are arranged as rows of a new matrix. This newly formed matrix will be referred to as the "feature matrix":

$$\lambda = [\lambda^1, \lambda^2, ..., \lambda^Q]. \quad (25)$$

Step 7: Finally, the "feature matrix" is multiplied by the "adjusted data matrix":

$$\psi = \lambda.\varsigma. \quad (26)$$

The rows of the resultant matrix ψ are the principal (uncorrelated) components in the data.

$$\psi = [\psi^1, \psi^2, ..., \psi^Q]. \quad (27)$$

The resultant components ψ^q are uncorrelated to each other. Therefore, the output of the PCA technique is a set of independent (uncorrelated) data of Q dimensions. These independent components are then treated as the data from separate measurement modes.

d. Implementation

The sequence of steps for evaluation of the posterior PDF of state (flaw depth) is shown in Figure 3, and is summarized below:

Step 1: Initialization: N_S samples are sampled at each position index from the prior PDF as given in equation (4).

Step 2: Weight Assignment: Weights are assigned using the likelihood PDF as indicated in equation (15). The likelihood PDF is represented by the error between the computed measurement using the measurement model and the actual measurement. As shown in figure 3, actual measurements (test data) and the computed measurement (using a

measurement model) are inputs to the weight assignment block. If the difference between computed and actual measurement for a sample (particle) is small, the likelihood or weight of sample is high, and vice versa. The measurement model typically relates the state to measurements and the results of inversion may be expected to depend on the choice of measurement model. The measurement model is derived from a training database of known states and corresponding NDE measurements. A comparative study using different measurement models to establish a relationship between the state and low frequency electromagnetic NDE measurements, in terms of accuracy of inversion and computational load, was carried out [44]. Based on the results reported in [44], the measurements (response) are approximated from the state through an R^{th}-order polynomial. The model is expressed as follows:

$$z_k = \sum_{r=0}^{R} c_r x_k^r \tag{28}$$

The coefficients of the polynomial c are determined from a training database of known states and corresponding measurements.

Step 3: Resampling: A common problem with particle filters is degeneracy [42], where after a few iterations, all but one particle will have negligible weight. The basic idea of resampling is to eliminate particles that have small weights and to concentrate on particles with large weights. The posterior PDFs (samples and associated weights) are estimated at all locations

Step 4: Convergence Check: Single point estimates of the unknown state are computed from the evaluated posterior PDF as described in Section 4a. The estimated posterior PDFs at all locations $(1:K)$ are then used as initial values and are updated iteratively (Figure 3). In subsequent iterations, the states (flaw depths) in the neighborhood of each location are the single point estimates from the PDFs evaluated at preceding iterations. The algorithm runs iteratively till the error between the single point flaw profile estimates in two consecutive iterations is less than some preset convergence criterion. If each iteration is denoted by I, and the estimated flaw depths throughout the specimen (*K* discretized locations) evaluated at I is $x_{1:K}(I)$, then the convergence criterion is given by

$$\frac{\sum_{k=1}^{K}(x_k(I+1)-x_k(I))^2}{K} \le \tau \,. \tag{29}$$

Here, τ is the preset convergence threshold. At convergence, $x_{1:K}(I+1)$ is assumed to be the predicted flaw profile.

The assumption of independence of measurement modes offers the foundation to the proposed particle filter based data fusion technique. As the output of PCA technique is a set of uncorrelated components, this transformation gives legitimacy to the assumption that measurement data is independent.

4. RESULTS

The proposed particle filter based technique was applied to steam generator tubing NDE data for flaw profiling, as well as for corrosion quantification in aircraft lap joints. Evaluation metrics are used to evaluate the performance of proposed inversion algorithm.

a. Evaluation Metrics

As discussed in the previous sections, the posterior PDF of the unknown quantity is evaluated at discrete positions using the proposed technique. *Posterior mean* and *maximum a posteriori* (MAP) estimates of the states at each location are subsequently computed from the posterior PDFs. These computed estimates are assumed to be the predicted flaw profiles in this study. The posterior mean estimate is given by

$$\hat{x}_{k|k}^{MMSE} = E\{x_k \mid z_k\} = \int x_k \, p(x_k \mid z_k) dx_k \tag{30}$$

while the *maximum a posteriori* (MAP) estimate is given as

$$\hat{x}_{k|k}^{MAP} = \max_{x_k} p(x_k \mid z_k) \tag{31}$$

The resulting predicted profiles using the PME and MAP estimates were compared with the true profiles using a mean-square error (MSE) metric [1]:

$$MSE = \frac{\sum_{k=1}^{K} (x_{k(predicted)} - x_{k(actual)})^2}{K}. \quad (32)$$

b. Steam Generator tubing NDE

The proposed technique is applied to estimate flaw profiles from multifrequency eddy current inspection [45] of steam generator (SG) tubing in nuclear power plants.

(i) Data Description

The experimental set up for eddy current testing is shown in figure 4 [45]. The setup includes steam generator (SG) tube along with motorized rotating probe coil (MRPC). The MRPC probe contains three coils, namely, a plus ('+') point coil, pancake coil and a high-frequency (HF) pancake coil. Measurements were acquired on tubes with laboratory-induced cracking, as well as tubes with cracking pulled from operational power plants. After the NDE measurements were acquired, the tubes were destructively analyzed, and the resulting metallographic (MET) results documenting the flaw depth profiles were used as "ground truth" in this study. Selected flaws from this database were used to formulate the training database from which the measurement model parameters were estimated. For evaluating the proposed algorithm performance, magnitude and phase of the complex eddy current data from the MRPC plus ('+') point probe, with excitation frequencies of 100 kHz, 200 kHz and 300 kHz, were used as the measurements.

(ii) Results

Twelve different defect profiles were selected from an industry test database for investigating the efficacy of the proposed inversion technique. The flaw profiles are tabulated in table 2. Only width and maximum depth are tabulated in the table. The number of samples used in the particle filter algorithm, at each position index, was 2000, while a 3rdorder polynomial measurement model was used. Three different values of the parameter L (0, 1 & 2), were used. The convergence threshold used in this study was $\tau = 10^{-3}$. Figure 5 shows the inversion results using data fusion of magnitude and phase measurement at 300 kHz for a flaw of width 7 mm and maximum depth of 100%

of tube wall thickness. Figures 5(a) and 5(b) shows phase and amplitude measurements respectively. Figures 5(c) and 5(d) shows top and 3-D views of computed posterior PDFs respectively. Figure 5(e) shows the computed estimates.

Figure 6 presents a summary of the MSE between PME and true flaw profiles for the twelve flaws, using different measurement modes and state vector length parameter $L = 0,1,2$. The MSE between PME and true flaw profile using measurement data at three individual frequencies (100, 200 and 300 kHz) are shown. The MSE between PME and true profiles using data fusion of measurement modes without PCA and with PCA are shown in figure 6. The average and standard deviation of MSE for each measurement mode are shown in figure 7.

b. Corrosion Quantification in Aircraft Lap Joints

(i) Data Description

Quantification of loss of plate thickness due to corrosion on aircraft skin is presented as a test case for 3-D flaw profile construction. The NDE measurement data was acquired from a 30-year old service-retired Boeing 727 aircraft as shown in figure 8. Two specimens (C and D), each consisting of a two-layer aluminum 2024-T3 lap joint cut out from below the cargo floor, were inspected. The thickness of each layer of the lap joint is 0.045 inches (1.143 mm). The specimens were disassembled and cleaned of all corrosion products after the inspection. X-ray mappings were then acquired to assess the true plate thickness. The inversion results were compared to the true thickness to determine the efficacy of the technique. Measurements from multiple frequency eddy current modes (5.5 kHz, 17 kHz and 30 kHz) were used in the inversion. The number of samples, N_s, in the particle filter was 2000. The resulting predicted profiles using posterior mean estimates and the MAP estimates are compared with the true profiles using a root mean-square error (RMSE) metric [46].

(ii) Results

The inversion result evaluated using a single measurement mode and fusing multiple measurement modes for specimen C is shown in figure 9. Results for specimen C and D are tabulated in table 3. Results indicate improvement in inversion accuracy when data fusion is used.

d. Discussion

Flaw depth profiling results from eddy current measurements indicate that the proposed particle filter approach is capable of producing reasonably accurate results, even in the presence of noise. In particular, results on experimental data validate the robustness of the proposed approach and indicate the feasibility of the proposed inversion technique. The use of data fusion is also seen to reduce the error in the reconstruction, when compared to flaw profiles obtained using a single measurement mode. The use of PCA further increases the accuracy of inversion. Note that in all cases, the flaw profile reconstructions were obtained using the particle filtering algorithm. Comparison with other contemporary techniques reported in the literature [46] indicates that the inversion results using particle filtering (with or without data fusion) are either comparable to or better than results obtained using these other techniques. The results also indicate that using a large neighborhood improves the inversion results. Note that the depth variation in real flaws can be abrupt, and flaw depth does not remain constant for long spans. This fact is a challenge for the proposed inversion technique. The use of a larger neighborhood (large value of L) appears to smooth out the variations in the flaw profiles and improves inversion accuracy. However, increasing the size of the neighborhood increases the computational cost. For instance, increasing L from 0 to 2 increases the computational load by a factor of five [47].

4. CONCLUSIONS & FUTURE WORK

A sequential Monte Carlo based data fusion technique was proposed for solving inverse problems. Results on multiple databases indicate the efficacy of proposed inversion technique. The proposed data fusion technique is based on the assumption that measurement processes are statistically independent processes, and the use of PCA was proposed to further legitimatize the assumption. The results indicate that the inversion results improve when data from multiple measurement modes is fused. Further improvement is observed in the inversion results when PCA is used prior to data fusion. Future work will focus on investigation of alternative preprocessing approaches when the assumption of independence is not valid. Application of the proposed technique on other

types of data sets is another focus area for future work. These data sets include X-ray tomography data and ultrasonic data.

REFERENCES

[1] T. Khan and P. Ramuhalli, "A Recursive Bayesian Estimation Method for Solving Electromagnetic NDE Inverse Problems," IEEE Transactions on Magnetics, vol. 44, no.7, pp.1845-1855, July2008.

[2] A. Tarantola, Inverse Problem Theory: Methods for Model Parameter Estimation, Elsevier, 1987.

[3] L. Udpa and S. Udpa, "Neural application of signal processing and pattern recognition techniques to inverse problems in NDE," Int. J. Appl. Electromagn. Mech., vol. 8, pp. 99–117, 1997.

[4] "A review of structural health monitoring literature: 1996–2001," Los Alamos National Laboratory, Tech. Rep. LA-13976-MS, 2003.

[5] P. Ramuhalli, L. Udpa, and S. Udpa, "Electromagnetic NDE signal inversion using function approximation neural networks," IEEE Trans. Magn., vol. 38, no. 6, pp. 3633–3642, Nov. 2002.

[6] P. Ramuhalli, L. Udpa, and S. Udpa, "Neural network algorithm for electromagnetic NDE signal inversion," in Electromagnetic Nondestruc.Eval. (V). Amsterdam, The Netherlands: IOS Press, 2001, pp. 121–128.

[7] M. Yan, M. Afzal, S. Udpa, S. Mandayam, Y. Sun, L. Udpa, and P. Sacks, "Iterative algorithms for electromagnetic NDE signal inversion," in ENDE (II), Series: Studies in Applied Electromagnetic and Mechanics, R. Albanese, G. Rubinacci, T. Takagi, and S. S. Udpa, Eds. Amsterdam, The Netherlands: IOS Press, 1998, vol. 14, pp. 287–296.

[8] S. Kirkpatrick, C. D. Gelatt, and M. P. Vecchi, "Optimization by simulated annealing," Science, vol. 220, no. 4598, pp. 671–680, May 13,1983.

[9] R. L. Haupt, "An introduction to genetic algorithms for electromagnetics," IEEE Trans. Antennas Propag., vol. 37, no. 2, pp. 7–15, Apr. 1995.

[10] S. Hoole, S. Subramanian, R. Saldanha, and J. Coulomb, "Inverse problem methodology and finite elements in the identification of cracks, sources, materials, and their geometry in inaccessible locations," IEEE Trans. Magn., vol. 27, no. 3, pp. 3433–3443, May 1991.

[11] K. Arunachalam, V. Melapudi, E. Rothwell, L. Udpa, and S. Udpa, "Microwave NDE for reinforced concrete," in Proc. Quant. Nondestruct. Eval., 2005.

[12] Z. Zeng, C. Lu, B. Shanker, and L. Udpa, "Element-free Galerkin method in modeling microwave inspection of civil structures," in Proc.12th Biennial IEEE Conf. Electromagn. Field Computation, 2006, vol. 27, pp. 268–1268.

[13] K. Arunachalam, "Investigation of a deformable mirror microwave imaging and therapy technique for breast cancer," Ph.D. dissertation, Michigan State Univ., East Lansing, 2006.

[14] Y. Kim, L. Jofre, F. D. Flaviis, and M. Q. Feng, "Microwave reflection tomographic array for damage detection of civil structures," IEEE Trans. Antennas Propag., vol. 51, no. 11, pp. 3022–3032, Nov. 2003.

[15] Y. Li et al., "An adjoint equation based method for 3D eddy current NDE signal inversion," in Electromagnetic Nondestruc. Eval. (V).Amsterdam, The Netherlands: IOS Press, 2001, pp. 89–96.

[16] Y. Li, L. Udpa, and S. Udpa, "Three dimensional defect reconstruction from eddy-current NDE signals using a genetic local search algorithm," IEEE Trans. Magn., vol. 27, no. 2, pp. 410–417, Mar. 2004.

[17] V. Monebhurrun, B. Duchene, and D. Lesselier, "3D inversion of eddy current data for nondestructive evaluation of steam generator tubes," Inverse Probl., vol. 14, pp. 707–724, 1998.

[18] M. Morozov, G. Rubinnaci, A. Tamburrino, and S. Ventre, "Numerical models of volumetric insulating cracks in eddy-current testing with experimental validation," IEEE Trans. Magn., vol. 42, no. 5, pp. 1568–1576, May 2006.

[19] S. Balasubramaniam, B. Shanker, and L. Udpa, "A fast integral equation based scheme for computing magnetostatic fields and its application to NDE problems," Proc. Quant. Nondestruct. Eval., vol. 20, pp. 331–337, 2001.

[20] R. Schifini and A. C. Bruno, “Experimental verification of a finite element model used in a magnetic flux leakage inverse problem,” J. Appl.Phys., vol. 38, pp. 1875–1880, 2005.
[21] S. Caorsi, G. L. Gragnani, S. Medicina, M. Pastorino, and G. Zunino, “Microwave imaging based on a Markov random field model,” IEEE Trans. Antennas Propag., vol. 42, no. 2, pp. 293–303, Mar. 1994.
[22] A. Dogandzic ,“Bayesian NDE defect signal analysis, IEEE Trans. Sig. Proc., 55,1,pg 372-378, 2007.
[23] A. Dogandzic and B. Zhang, “Markov chain Montecarlo defect identification in NDE images,” Review of Progress in Quantitative Nondestructive, 2007.
[24] Z.Liu et al, “Survey: State of the art in NDE data fusion techniques,” IEEE Trans. Instrum. Meas., vol. 56, no.6, pp2435-2451, Dec 2007.
[25] X.E.Gross, NDT Data Fusion, Butterworth-Heinemann, Boston (1997).
[26] J. Yim, S. S. Udpa, M. Mina, and L. Udpa, “Optimum filter based techniques for data fusion,” in Review of Progress in QNDE, vol. 15,D. O. Thompson and D. E. Chimenti, Eds. New York: Plenum, 1996, pp. 773–780.
[27] J. Yim, S. S. Udpa, L. Udpa, and W. Lord, “Neural network approaches to data fusion,” in Review of Progress in QNDE, vol. 14, D. O. Thompson and D. E. Chimenti, Eds. New York: Plenum, 1995, pp. 819–826.
[28] G. Simone and F. C. Morabito, “NDT image fusion using eddy current and ultrasonic data,” Int. J. Comput. Math. Elect. Electron. Eng., vol. 20, no. 3, pp. 857–868, 2001.
[29] J. Dion, M. Kumar and P. Ramuhalli, “ Multi-sensor data fusion for high-resolution material characterization,” in Review of Progress in QNDE, AIP Conference Proceedings vol. 894, pp. 1189-1196.
[30] X. E. Gros, P. Strachan, and D. W. Lowden, “Theory and implementation of NDT data fusion,” Res. Nondestruct. Eval., vol. 6, no. 4, pp. 227–236, Dec. 1995.
[31] X. E. Gros, Z. Liu and K. Hanasaki, “Experimenting with pixel level NDT data fusion techniques,” IEEE Trans. Instrum. Meas., vol. 49, no. 5, pp. 1083–1090, Oct. 2000.
[32] V. Kaftandjian and N. Francois, “Use of data fusion methods to improve reliability of inspection: Synthesis of the work done in the frame of a European thematic network,” in Proc. 8thECNDT , Barcelona, Spain, Jun. 2002, vol. 8. NDT. net, no. 2.
[33] Z. Liu et al, “One-dimensional eddy current multi-frequency data fusion: A multi-resolution analysis approach,” Insight, vol. 40, no. 4, pp. 286–289, Apr. 1998.
[34] Y. W. Song and S. S. Udpa, “A new morphological algorithm for fusing ultrasonic and eddy current images,” in Proc. IEEE Ultrason. Symp.,1996, pp. 649–652.
[35] Z. Liu et al, “3D visualization of ultrasonic inspection data by using AVS,” in Proc. 5thFar-East Conf. Nondestructive Testing, Kenting, Taiwan, R.O.C., Nov. 1999, pp. 549–554.
[36] D.S. Forsyth et al, “The role of data fusion in NDE for aging aircraft,” Proc. SPIE, vol.3394, pp.47-58, 2000.
[37] K. Sun et al, “Registration issues in the fusion of eddy current and ultrasonic NDE data using Q-transforms,” in Review of Progress in QNDE, vol. 15, D. O. Thompson and D. E. Chimenti, Eds. New York: Plenum, 1996, pp. 813–820.
[38] G. Givens and J. Hoeting, Computational Statistics, Wiley Series, 2005.
[39] A. Tamburrino, “A communication theory approach for electromagnetic inverse problems,” *IEEE Trans. Magn.*, vol. 36, pp. 1136–1139, 2000
[40] N. Alves, “Ising model Monte Carlo simulations: density of states and mass gap”, Phys. Rev. B 41 383.1990.
[41] B. Ristic, S. Arulampalam and N. Gordon, Beyond the Kalman Filter. London, U.K.: Artech House, 2004.
[42] S. Arulampalam, S. Maskell, N. Gordon, and T. Clapp, “A tutorial on particle filters for on-line non-linear/non-Gaussian Bayesian tracking,”IEEE Trans. Signal Process., vol. 50, pp. 174–189, 2002.
[43] I. T. Jolliffe, Principal component analysis, Springer 2002.
[44] T. Khan and P. Ramuhalli, “Sequential Monte Carlo Methods for Electromagnetic NDE Inverse Problems—Evaluation and Comparison of Measurement Models,” IEEE Trans. Mag. Vol. 45, 3, pp. 1566-1569, 2009.

[45] J. R. Bowler, Review of eddy current inversion with application to nondestructive evaluation, Int. J. Appl Electromagn. Mech. 8: 3-16 1997

[46] Z. Liu, et al., “Combining multiple nondestructive inspection images with a generalized additive model,” Measurement Science and Technology, Vol. 19, No. 8, August 2008.

[47] T. Khan, “A sequential Monte carlo based recursive technique for solving NDE inverse problems,” Ph.D. dissertation, ECE, MSU, East Lansing, MI, 2009.

LIST OF FIGURES

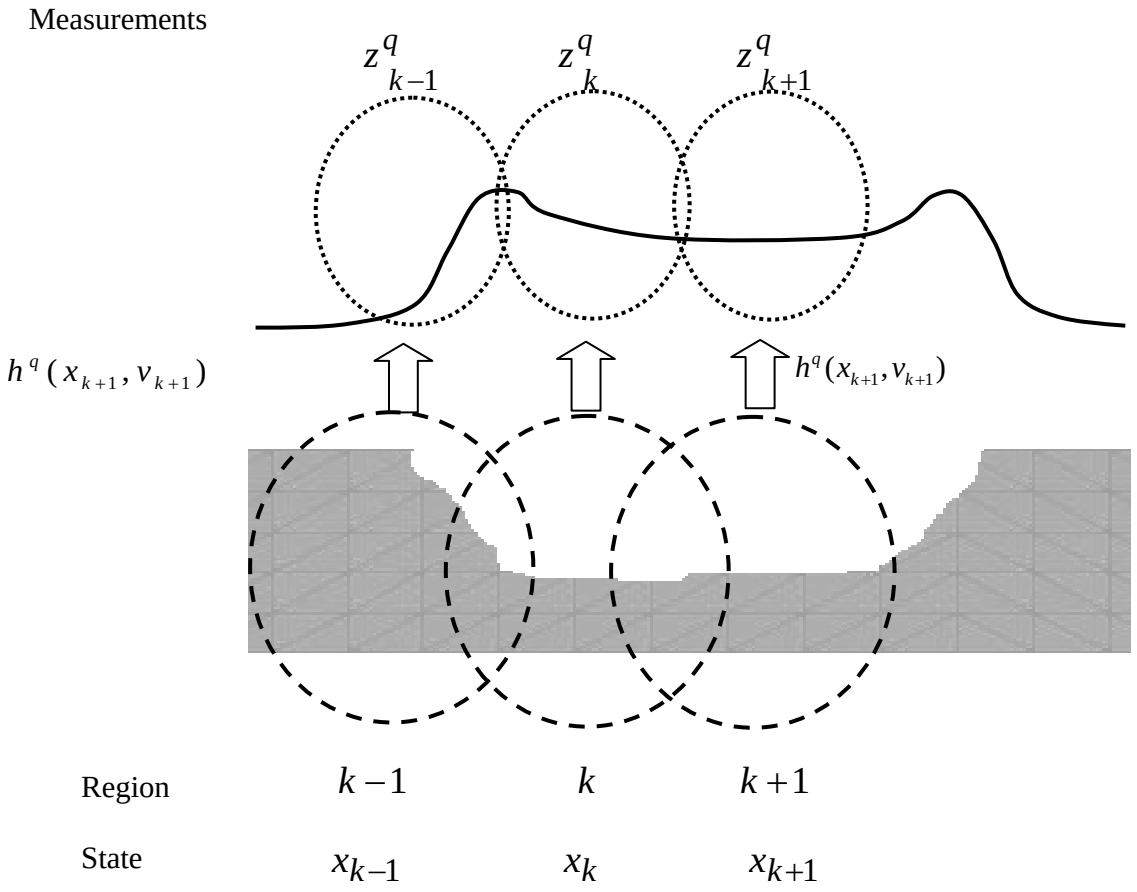
Measurements
z^q_{k-1}
z^q_k
z^q_{k+1}
$h^q(x_{k+1}, v_{k+1})$
$h^q(x_{k+1}, v_{k+1})$
Region
$k-1$
k
$k+1$
State
x_{k-1}
x_k
x_{k+1}

Figure1

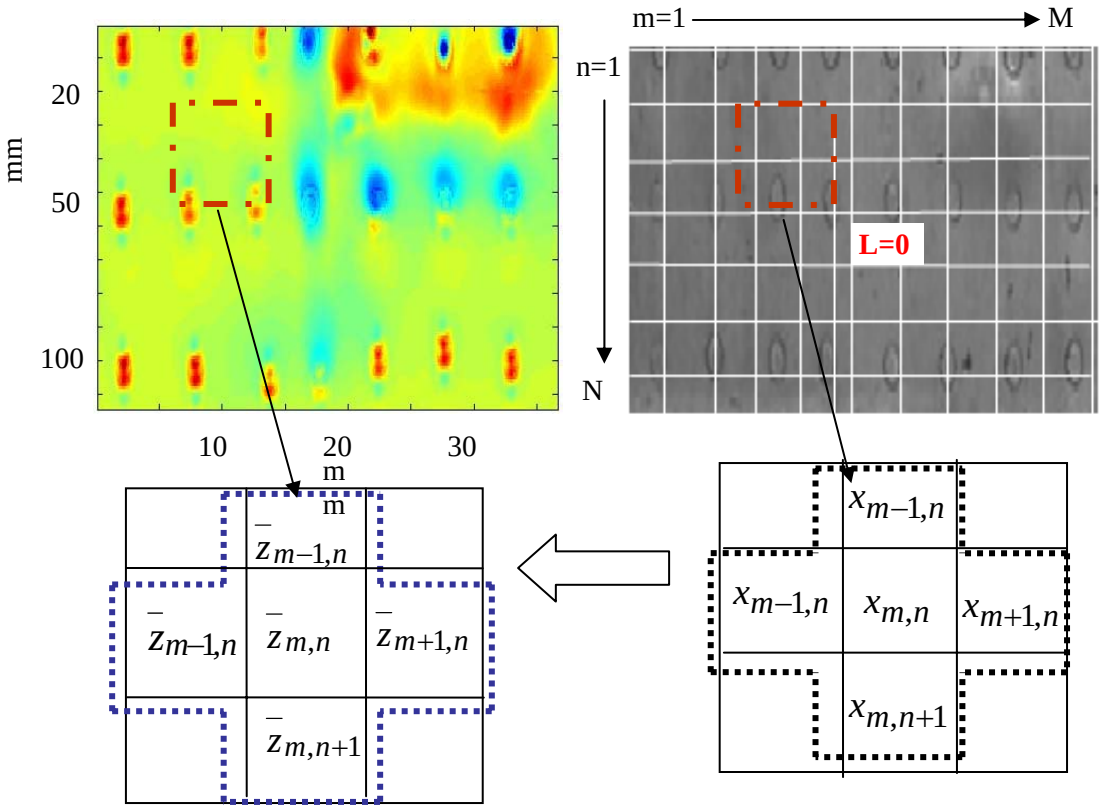
m=1
M
n=1
N
mm
20
50
100
10
20
30
m
L=0
$\bar{z}_{m-1,n}$
$\bar{z}_{m-1,n}$
$\bar{z}_{m,n}$
$\bar{z}_{m+1,n}$
$\bar{z}_{m,n+1}$
$x_{m-1,n}$
$x_{m-1,n}$
$x_{m,n}$
$x_{m+1,n}$
$x_{m,n+1}$

Figure2

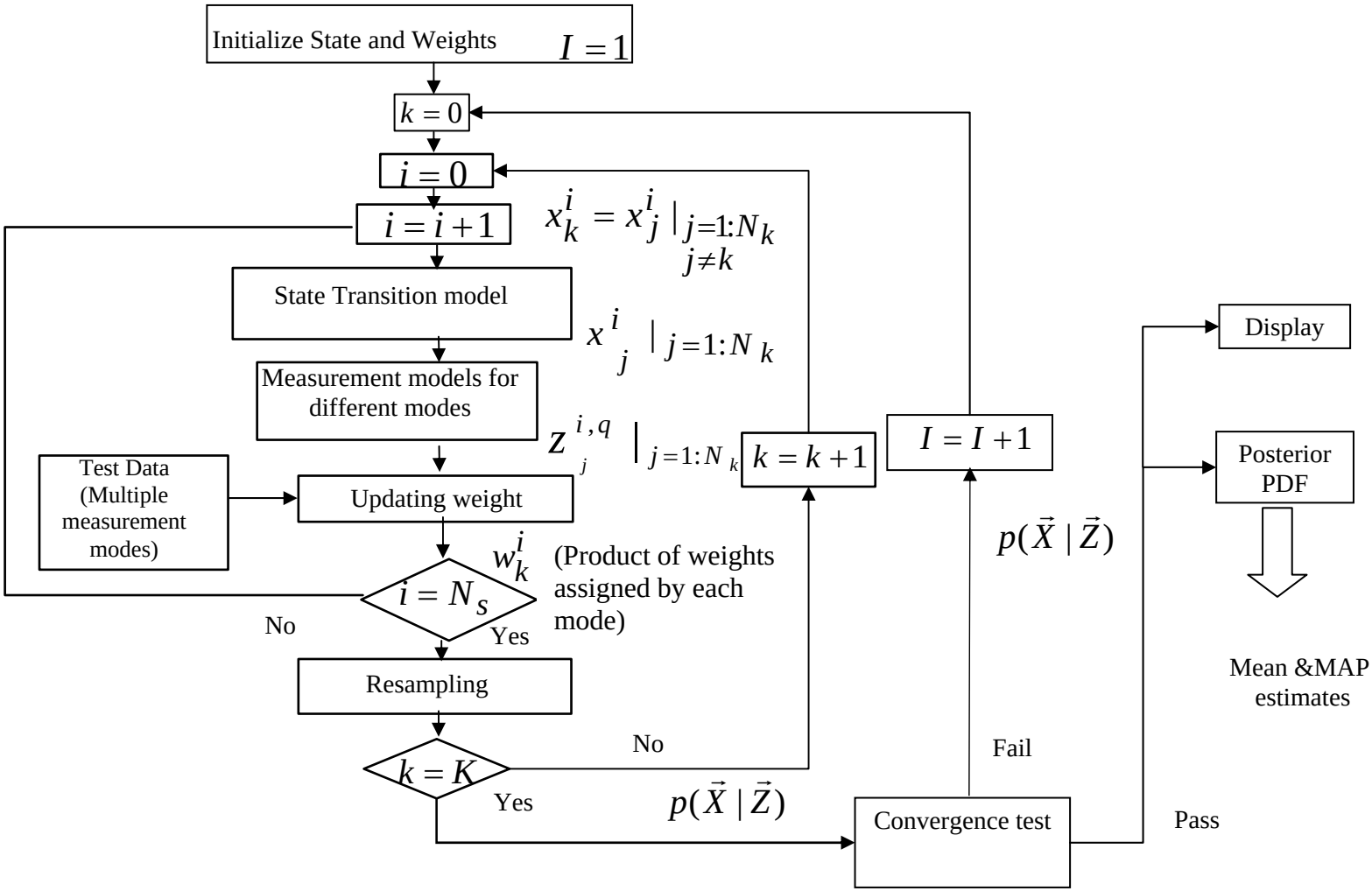
Initialize State and Weights
$I = 1$
$k = 0$
$i = 0$
$i = i + 1$
$x_k^i = x_j^i \mid_{\substack{j=1:N_k \\ j \neq k}}$
State Transition model
$x_j^i \mid_{j=1:N_k}$
Measurement models for different modes
$z_j^{i,q} \mid_{j=1:N_k}$
Test Data (Multiple measurement modes)
Updating weight
w_k^i
(Product of weights assigned by each mode)
$i = N_s$
No
Yes
Resampling
$k = K$
No
Yes
$k = k + 1$
$I = I + 1$
$p(\vec{X} \mid \vec{Z})$
$p(\vec{X} \mid \vec{Z})$
Convergence test
Fail
Pass
Display
Posterior PDF
Mean &MAP estimates

Figure 3

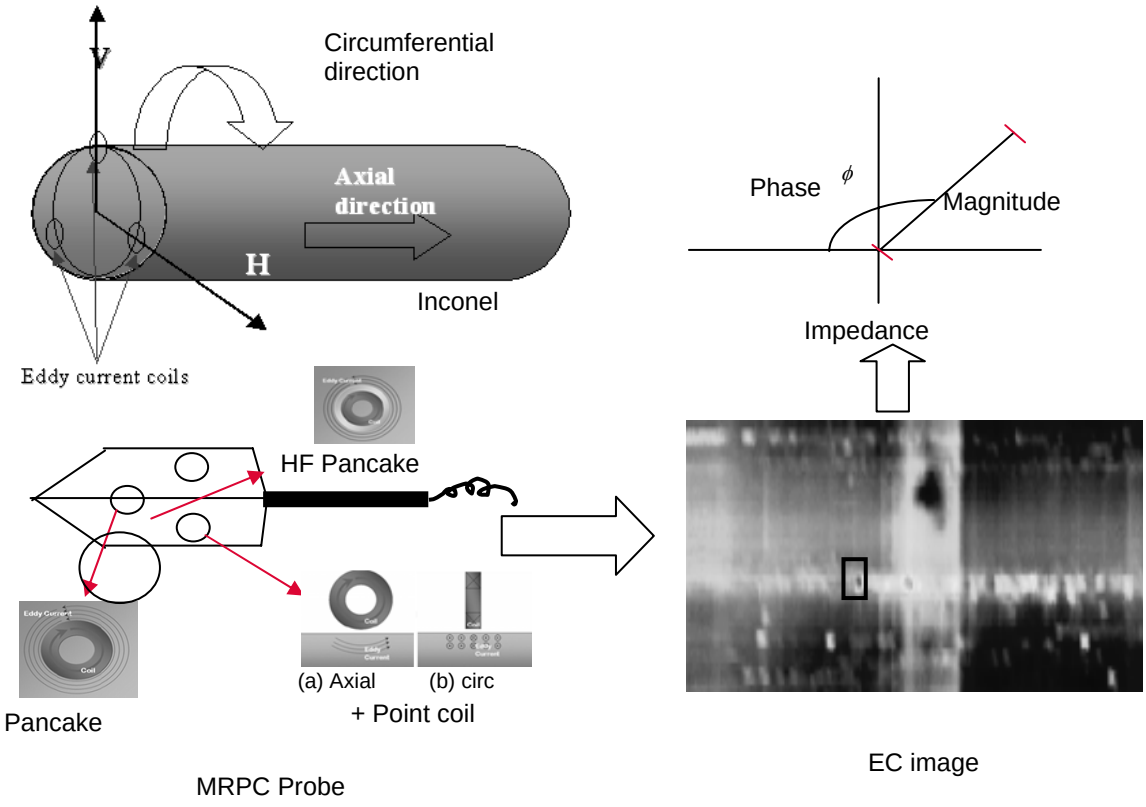
V
Circumferential direction
Axial direction
H
Inconel
Eddy current coils
HF Pancake
Pancake
(a) Axial
(b) circ
+ Point coil
MRPC Probe
Phase
ϕ
Magnitude
Impedance
EC image

Figure 4

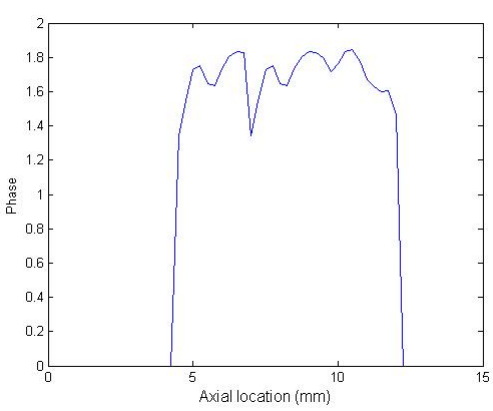

(a)

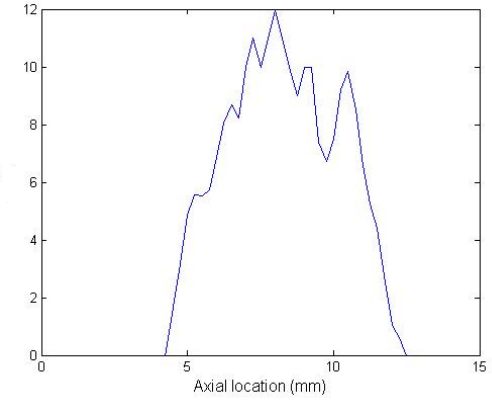

(b)

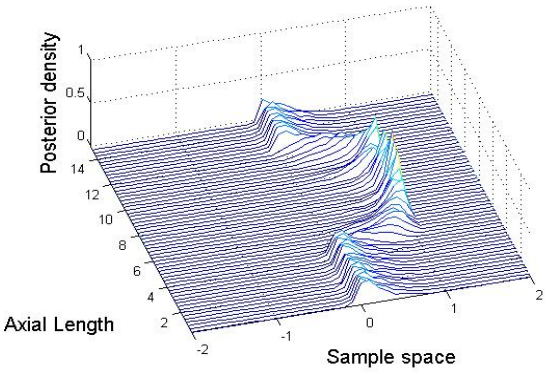

(c)

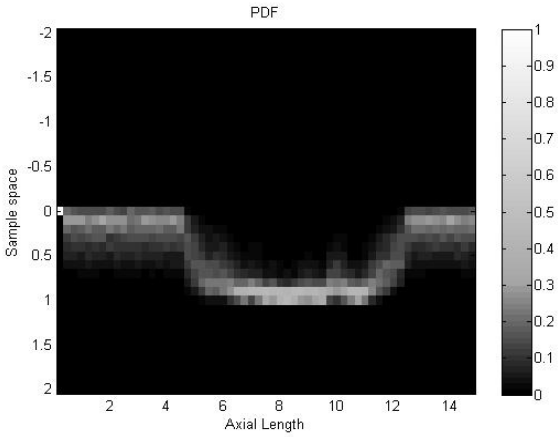

(d)

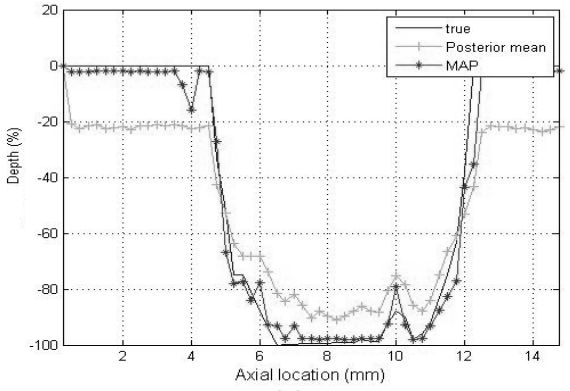

(e)

Figure 5

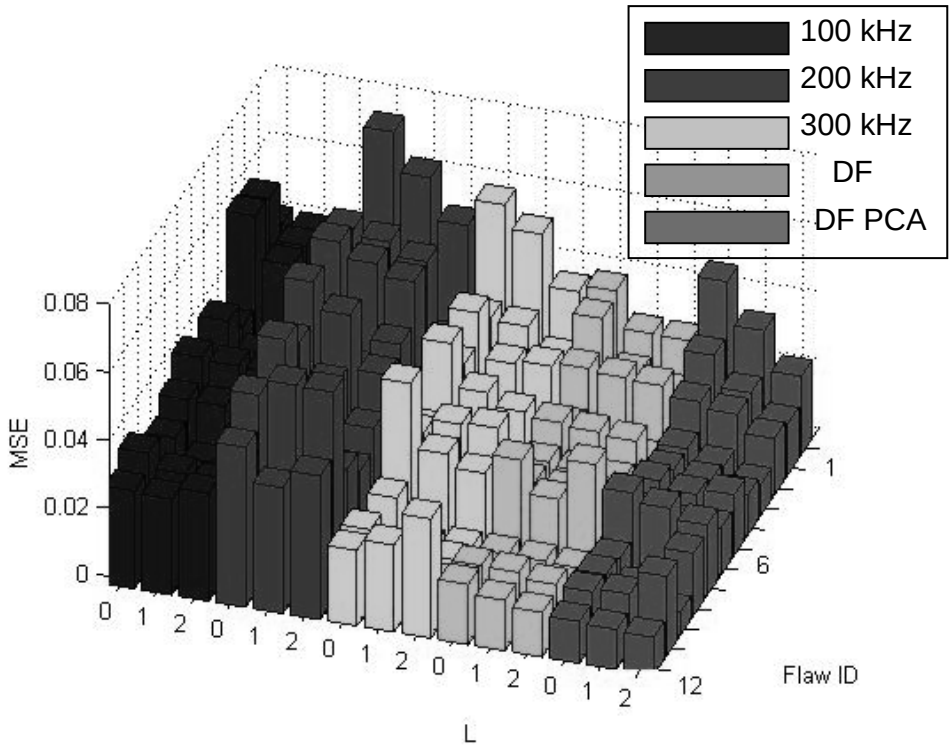
100 kHz
200 kHz
300 kHz
DF
DF PCA
MSE
0.08
0.06
0.04
0.02
0
0 1 2 0 1 2 0 1 2 0 1 2 0 1 2
L
1
6
12
Flaw ID

Figure 6

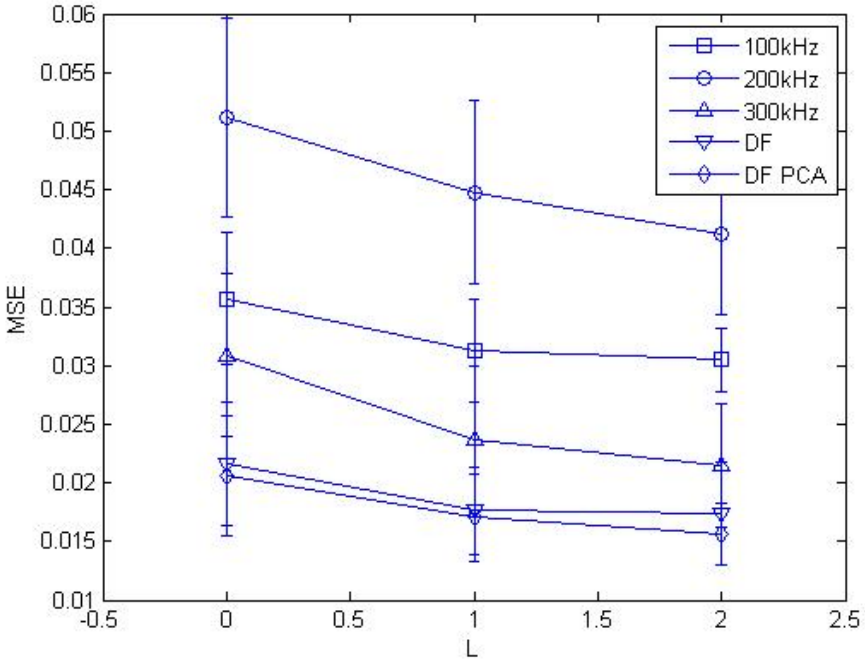
0.06
0.055
0.05
0.045
0.04
0.035
0.03
0.025
0.02
0.015
0.01
MSE
-0.5
0
0.5
1
1.5
2
2.5
L
100kHz
200kHz
300kHz
DF
DF PCA

Figure 7

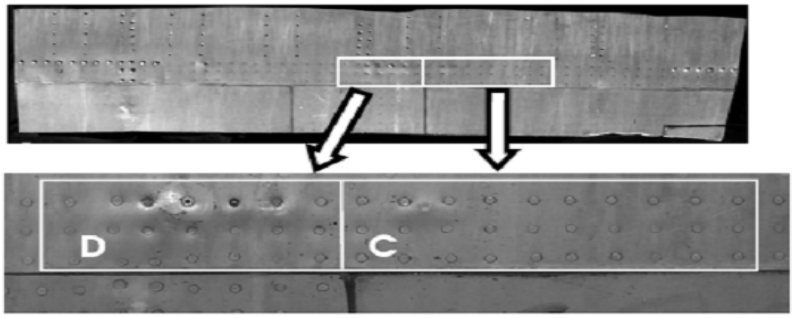

Figure 8

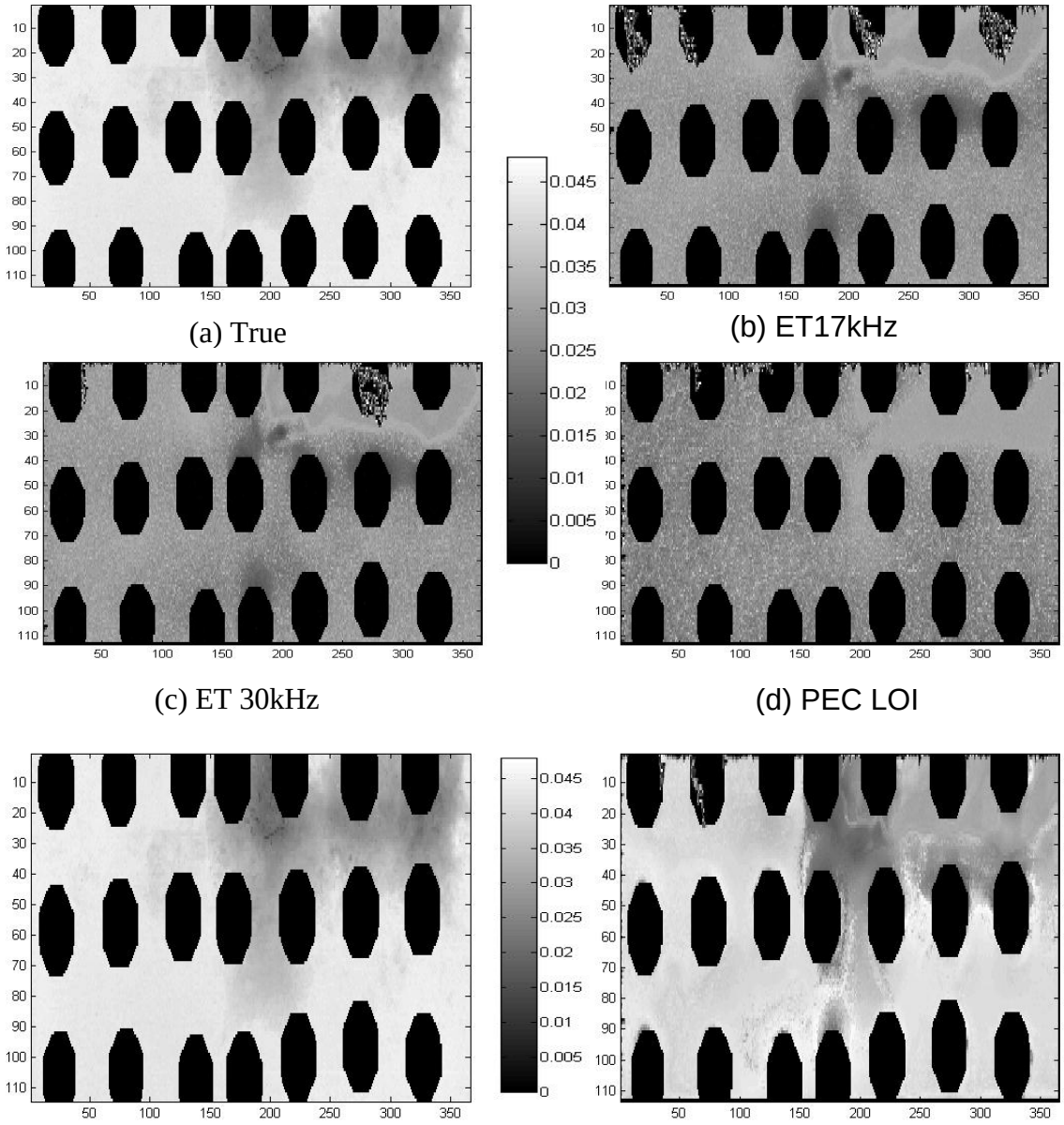

(a) True (b) ET17kHz

(c) ET 30kHz (d) PEC LOI

(e) True (f) Data Fusion

Figure 9

List of Tables

Table 1

Notation	Description
k	Discretized location
x_k	Flaw depth at location k (State)
z_k	NDE measurement at location k
K	Total number of discretized locations
q	Measurement mode
Q	Total number of measurement modes
$\bar{z}_k$	Set of measurements at location k due to all measurement modes
$\vec{Z}$	Set of measurements corresponding to all measurement modes Q at all locations K
$\vec{X}$	Set of states (flaw depths)
N_k	Elements in the neighborhood of location k
L	Parameter controlling size of neighborhood
x_k^i	i^{th} Sample (particle) at location k
$w_k^{i,q}$	Weight assigned to x_k^i by *qth* measurement mode
N_s	Total number of samples (particles)
I	No. of iteration
τ	Preset convergence threshold
c	Measurement model r-th coefficient
R	Order of polynomial measurement model
$x_{k\|k}^{MMSE}$	Posterior mean estimate
$x_{k\|k}^{MAP}$	Maximum a posteriori estimate
MSE	Mean square error
RMSE	Root Mean square error

Table 2

Flaw ID	1	2	3	4	5	6	7	8	9	10	11	12
Width (mm)	2.75	7.00	5.50	3.00	2.75	2.25	5.25	11.00	2.50	3.00	3.25	3.50
% Max Depth	20	100	100	85	90	70	78	60	58	71	39	76

Table 3

S.No	Measurement mode	RMSE (X10-3)	
		Section C	Section D
1.	17 kHz Eddy Current	3.19	4.31
2.	30 kHz Eddy Current	2.96	3.82
3.	P-ET LOI	3.89	5.13
4.	Data Fusion (17kHzET+30kHzET+P-ET LOI)	1.86	2.21